Influence of fiber misalignments on buckling performance of variable stiffness composites using layerwise models and random fields

Influence of fibre misalignments on buckling performance of variable stiffness composites using layerwise models and random fields

A. Pagani*, A. R. Sanchez-Majano

Mul^2 Team
Department of Mechanical and Aerospace Engineering, Politecnico di Torino
Corso Duca degli Abruzzi 24, 10129 Torino, Italy.

Abstract: *Additive manufacturing brought to the emergence of a new class of fibre-reinforced materials; namely, the Variable Angle Tow (VAT) composites. Automated fibre placement machines allow the fibres to be relaxed along curvilinear paths within the lamina. In theory, the designer can conceive VAT structures with unexplored capabilities and tailor materials with optimized stiffness-to-weight ratios. In practise, steering brittle fibres, generally made of glass or carbon, is not trivial and highly affected from the printer signature. This paper wants to explore the effect of fibre misalignment on the buckling response of laminated VAT composites. For doing so, we use the Carrera Unified Formulation (CUF), which allows to develop layerwise models with unprecedented accuracy in a straightforward and systematic manner. Variation patterns are generated at the layer scale by means of random fields through a Monte Carlo analysis. The stochastic variation (defects) is propagated through the scales and correlated with the global buckling response of VAT panels. The results show that layerwise models outperform equivalent single layer theories, since the former are able to foresee eventual switching between buckling modes, and thus making them fundamental in uncertainty analysis.*

Keywords: Variable angle tow composites, Defect sensitivity, Uncertainty analysis, Carrera unified formulation.

---

1 Introduction

Composite materials are greatly known for their ability to change the stiffness and strength properties by opportunely designing the laminate layup sequence. The capability of retrieving the better performing stack of a laminate that is a constituent of a certain structural component subjected to specified loads is commonly known as tailoring. For instance, a classic tailoring problem is to determine the layup sequence of a laminated composite panel with specified boundary conditions, geometrical properties and applied loads that maximizes the buckling performance whilst preserving the load-carrying capability without failures [1].

*Corresponding author. E-mail: alfonso.pagani@polito.it

Traditionally, that kind of tailoring is done by keeping the fibre orientation constant within each layer throughout a structural component. Nevertheless, straight-fibre composites (i.e., constant stiffness composites) cannot address efficiently optimisation problems when the actual internal stress distribution is non-uniform (hence leading to non-uniform resultants, N_x, N_y and N_{xy}) within the component. A classic example of component configuration with highly non-uniform stress distribution is the panel with a hole. In such a case, if each layer is limited to a single orientation over the whole component, the designer will be incapable to fully take advantage of the directional material properties offered by advanced composites, ever since the design will be driven by the location that presents the most critical stress state. A comprehensive study on this topic was conducted by Biggers [2, 3], where tailoring was achieved by redistributing the layers with specified orientations across the planform of rectangular plates to create beneficial stiffening patterns against compression and shear buckling.

Many studies by Banichuk [4, 5], Pedersen [6, 7] and Duvaut [8] concerned spatial variation of fibre orientation within the domain of a composite panel to improve some structural performance. However, the feasibility or practicality of actual fabrication of the resulting designs were not taken into account. It was in the works by Olmedo and Gürdal [9, 10, 11] when an effort to integrate realistic fabrication techniques into the design of laminates with curvilinear fibre layers was achieved. The proposed fibre path was intended to be used with state of the art manufacturing techniques for composite laminates, such as automated fibre placement (AFP) that allow the fibres to be steered and vary the fibre orientation angle within the layer as a function of the position throughout the structure. Stiffness properties, such as longitudinal and transverse moduli, depend on the local fibre orientation angle. Consequently, a curvilinear fibre path will present variable stiffness properties conversely to a traditional straight-fibre layer that shows constant stiffness properties within the plane.

In the aforementioned works, certain manufacturing constraints, such as the minimum turning radius, which determines the maximum amount of steering that is possible with an AFP machine, were not considered. Therefore, not all the solutions obtained could be manufactured exploiting the capabilities of AFP machine. Additionally, due to the manufacturing features inherent to AFP, laminates are not exempt from flaws; certain defects such as gaps, overlaps and fibre misalignments often appear in the final structure, and hence affecting the structural performance as demonstrated by Blom *et al.* [12], where the influence of tow-drop areas on the strength and stiffness of VAT plates was characterised. Moreover, works by Fayazbakhsh *et al.* [13] and Nik *et al.* [14] showed that a complete gap strategy leads to lower buckling and in-plane stiffness whereas complete overlap strategy outperforms the defect-free structure in such terms. Additionally, Wu *et al.* [15] conducted buckling analyses which showed for two tow-steered shells that VAT composites may offer great potential for reducing the detrimental impact of geometric imperfections on structural performance.

In this paper, VAT plates are modelled using Carrera Unified Formulation (CUF), which allows to develop structural models with scalable accuracy in a straightforward and systematic manner, as proven in works by Carrera [16], Carrera and Giunta [17], Carrera *et al.* [18, 19]. CUF has been recently extended to the study of VAT laminates. For instance, Demasi [20, 21] employed equivalent single layer, zig-zag and layerwise theories for the through-the-thickness discretization of the displacement variables to perform static analyses and showed the versatility of CUF against commercial software. On the other hand, Viglietti *et al.* [22] introduced 1D models, where the cross-section behaviour was described using equivalent single layer and layerwise expansions, in order to perform free vibration analyses of VAT structures. Those works demonstrated that layerwise models provide the most accurate solutions in comparison with 3D models, while presenting a strong reduction in the number of degrees of freedom.

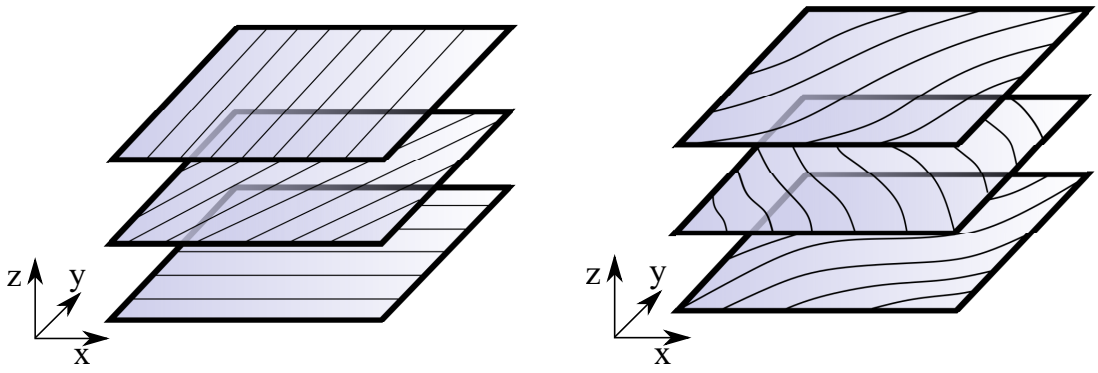

(a) Straight-fibre laminate (b) VAT laminate

Figure 1: Comparison of stacking sequences between classical straight-fibre and VAT laminates.

Another advantage of layerwise formulation is that they are able to model the meso-scale behaviour of composite laminates, thus fabrication flaws such as printing defects can be taken into account.

In this context, uncertainty analysis employing Monte Carlo simulations and CUF-based layerwise models of VAT laminates subjected to meso-scale fibre misalignments defects are carried out. The printing defects are modelled by stochastic fields, where a certain misalignment spatial distribution and standard deviation are assumed. The field of stochastic variations has been fruitfully studied, yielding a plethora of methods for the study of stochastic structural mechanics as depicted in the review by Schüeller [23]. One of these techniques is the Stochastic Finite Element method which is an extension of the classical deterministic Finite Element approach to the stochastic framework, i.e. to the solution of static and dynamic problems with stochastic mechanical, geometric and/or loading properties [24]. Uncertainty analysis has been demonstrated to be a significant aspect of the design process, as showed by Mukherjee *et al.* [25], after using Tsai-Wu failure envelopes as a constraint in the minimum weight design of a composite laminate. Particularly, in this research we use a methodology similar to the demonstrated by Scarth *et al.* [26], who employed random fields to model the variability of the mechanical properties of the materials used in an aircraft wing to characterise its free vibration response.

The manuscript is organized as follows: Section 2 describes the constitutive behaviour of VAT composite laminates. In Section 3, CUF-based theories of structures based on equivalent single layer (ESL) and layerwise (LW) strategies are discussed along with an opportune finite element solution. Then, Section 4 describes how the random field that represents the fibre misalignments is generated. Finally, Section 5 presents the outcomes of the carried out simulations combined with the statistical treatment of the critical buckling loads and modes.

2 Variable Stiffness Composites

Unlike classical composites where fibres relax along a fixed direction at each lamina, thus yielding a constant stiffness per ply, in variable angle tow composites the fibres are allowed to vary along a curvilinear pattern within each lamina, see Fig. 1, and therefore providing a variable stiffness in the plane. In this work, the fibre orientation θ is defined following the notation described in previous works by Gürdal [11], where the fibre path presents a rotation of an angle ϕ with regard to a certain reference direction placed at an arbitrary point A as shown in Fig. 2. The fibre orientation angle at this point is T_0 and varies along

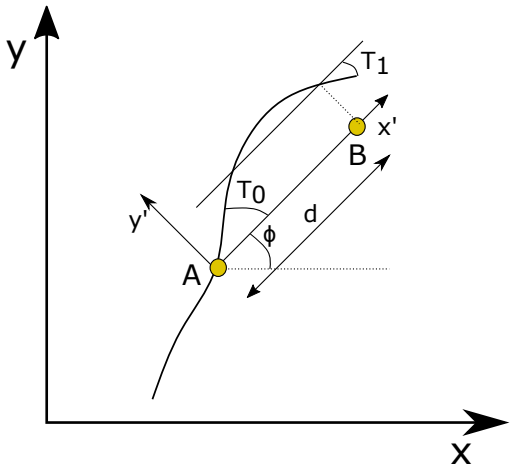

Figure 2: Reference path definition of a variable angle orientation layer.

a direction x' oriented by angle ϕ from the original coordinate axis x. The fibre orientation is assumed to reach a value T_1 at a characteristic distance d from the reference point. By introducing this rotation angle, the fibre orientation path $\theta(x, y)$ can be expressed as $\theta(x')$, where $x' = x\cos\phi + y\sin\phi$. With a linear variation of the fibre orientation angle between points A and B, the equation of the fibre orientation along this reference path takes the form:

$$\theta(x') = \phi + T_0 + \frac{(T_1 - T_0)}{d}|x'| \tag{1}$$

In classic straight-fibre laminates, each lamina is defined by a single angle. Note that for VAT laminates employing a linear variation there are three angles and a characteristic length. Although, the representation of a single curvilinear ply might be $[\phi < T_0, T_1 >]$, because the characteristic distance is assumed to be associated to a geometric property. In the literature related to VAT laminates, d commonly equals $a/2$ or $b/2$ respectively when $\phi = 0°$ or $\phi = 90°$, where a is the width and b is the length of the plate.

Independently of the fibre orientation angle, the three-dimensional constitutive behaviour of a composite ply made of linear elastic material can be expressed with the generalised Hooke law. In the material reference system, it reads:

$$\boldsymbol{\sigma} = \mathbf{C}\boldsymbol{\varepsilon} \tag{2}$$

In Eq. (2), $\boldsymbol{\sigma}$ and $\boldsymbol{\varepsilon}$ are the stress and strain vectors expressed in the Voigt notation. Furthermore, $\mathbf{C}$ is the material stiffness matrix, which is symmetric and contains nine independent terms in the case of orthotropic material. When a VAT lamina is considered, the fibre orientation is a function of the plane coordinates, i.e. $\theta(x, y)$. As a consequence, in a generic Cartesian reference system, the Hooke law will read:

$$\boldsymbol{\sigma} = \widetilde{\mathbf{C}}(x, y)\boldsymbol{\varepsilon} \tag{3}$$

where

$$\widetilde{\mathbf{C}}(x, y) = \mathbf{T}(x, y)\mathbf{C}\left(\mathbf{T}(x, y)\right)^T \tag{4}$$

The apex "T" denoted transposition. The rotation matrix $\mathbf{T}$ (and consequently $\widetilde{\mathbf{C}}$) is constant within the ply in the case of classical laminates, whereas it changes point-wise in VATs. This matrix is not reported here for the sake of brevity, but it can be found in many reference texts, see for example [27].

3 Layerwise models of VAT panels

3.1 Carrera unified formulation

In this paper, VAT composites structures are modelled using refined 1D CUF models, which have been demonstrated to provide accurate results for any geometry and material anisotropy, see [28]. In the CUF framework, the generic 3D displacement field can be expressed as an arbitrary expansion of the 1D generalised unknowns which lay along the y-axis, i.e:

$$\mathbf{u}(x,y,z) = F_\tau(x,z)\mathbf{u}_\tau(y) \quad \tau = 1,2,...,M \tag{5}$$

in which $\mathbf{u}_\tau(y)$ is the vector of the general displacements, M is the number of the expansion terms and $F_\tau(x,z)$ is an arbitrary cross-section expansion depending on x and z. Note that different classes of 1D structural theories can be implemented by opportunely choosing the $F_\tau(x,z)$ functions. In this manuscript, the so-called Taylor Expansion (TE) and Lagrange Expansion (LE) CUF-based 1D models are adopted. For different classes of structural theories, interested readers are referred to [29, 30, 31].

3.1.1 Taylor expansions

TE models make use of 2D polynomials of the type $x^i z^j$ as $F_\tau(x,z)$. It is important to underline that the kinematic fields of many classical beam theories (e.g., Euler-Bernouilli and Timoshenko) can be defined as particular cases of the first order TE model (TE1), which reads:

$$\begin{aligned} u_x &= u_{x1} + xu_{x2} + zu_{x3} \\ u_y &= u_{y1} + xu_{y2} + zu_{y3} \\ u_z &= u_{z1} + xu_{z2} + zu_{z3} \end{aligned} \tag{6}$$

Higher-order models can be obtained by adding terms to the displacement field of Eq. (6) in a hierarchical manner [32].

3.1.2 Lagrange expansions

In the case of LE, Lagrange polynomials are used as generic functions above the cross-section. Thus, the cross-section is divided into a certain number of local expansion sub-domains, whose polynomial degree depends on the sort of Lagrange expansion employed. Three-node linear L3, four-node bilinear L4, nine-node quadratic L9 and sixteen-node L16 polynomials can be used, for example, to formulate refined beam theories (see Carrera and Petrolo [33]). As an example, the interpolation functions of a L9 expansion set are defined as:

$$\begin{aligned} F_\tau &= \tfrac{1}{4}(r^2 + rr_\tau)(s^2 + ss_\tau) \text{ if } \tau = 1,3,5,7 \\ F_\tau &= \tfrac{1}{2}s_\tau^2(s^2 - ss_\tau)(1-r^2) + \tfrac{1}{2}r_\tau^2(r^2 - rr_\tau)(1-s^2) \text{ if } \tau = 2,4,6,8 \\ F_\tau &= (1-r^2)(1-s^2) \text{ if } \tau = 9 \end{aligned} \tag{7}$$

where r and s range from -1 to +1, and r_τ and s_τ represent the locations of the roots. Therefore, the kinematic field of the single-L9 beam theory can be expressed as:

$$\begin{aligned} u_x &= F_1u_{x1} + F_2u_{x2} + F_3u_{x3} + F_4u_{x4} + F_5u_{x5} + F_6u_{x6} + F_7u_{x7} + F_8u_{x8} + F_9u_{x9} \\ u_y &= F_1u_{y1} + F_2u_{y2} + F_3u_{y3} + F_4u_{y4} + F_5u_{y5} + F_6u_{y6} + F_7u_{y7} + F_8u_{y8} + F_9u_{y9} \\ u_z &= F_1u_{z1} + F_2u_{z2} + F_3u_{z3} + F_4u_{z4} + F_5u_{z5} + F_6u_{z6} + F_7u_{z7} + F_8u_{z8} + F_9u_{z9} \end{aligned} \tag{8}$$

Refined beam models can be obtained by adopting higher order Lagrange polynomials or by using a combination of Lagrange polynomials on multi-domain cross-section. Further information on LE models can be found in [29, 30]. Note that LE models employ pure displacement unknowns. This aspect makes LE particularly advantageous in the implementation of layerwise models, because interlaminar displacements continuity can be satisfied automatically, see Section 3.1.4.

3.1.3 Finite element approximation

Various numerical methods can be used along with CUF to solve 1D to 3D problems. The finite element (FE) formulation has been selected in the present work due to its advantages in the study of arbitrary geometries and boundary conditions. The generalized displacements are in this way described as functions of the unknown nodal vector $\mathbf{u}_{\tau i}$ and the shape functions N_i; i.e.,

$$\mathbf{u}_\tau(y) = N_i(y)\mathbf{u}_{\tau i} \quad i = 1, 2, ..., N_{elem} \tag{9}$$

where N_{elem} is the number of nodes per element. Different sets of polynomials can be used to define FEs. Lagrange interpolation polynomials have been chosen in this work to generate cubic one-dimensional elements. This expressions are not included for the sake of brevity, but they can be found in the book by Carrera *et al.* [32], in which two-node (B2), three-node (B3) and four-node (B4) elements are described. Finally, by introducing Eq. (9) into Eq. (5), the displacement field results:

$$\mathbf{u}(x, y, z) = F_\tau(x, z)N_i(y)\mathbf{u}_{\tau i} \quad \tau = 1, 2, ..., M \;\; i = 1, 2, ..., N_{elem} \tag{10}$$

The resolution of the buckling problem is realized by seeking bifurcations and limit points in the equilibrium state:

$$|\mathbf{K}_T| = 0 \tag{11}$$

$\mathbf{K}_T$ is the tangent stiffness matrix of the structure. This matrix is obtained by means of the principle of virtual displacements as follows:

$$\delta^2(L_{int}) = \int_V \delta(\delta\boldsymbol{\varepsilon}^{\boldsymbol{T}}\boldsymbol{\sigma})\, dV = \int_V \left(\delta\left(\delta\boldsymbol{\varepsilon}^{\boldsymbol{T}}\right)\boldsymbol{\sigma} + \delta\boldsymbol{\varepsilon}^{\boldsymbol{T}}\delta\boldsymbol{\sigma}\right)\, dV \tag{12}$$

where L_{int} is the internal strain energy and δ denotes the virtual variation. After substituting CUF and FEM approximations (Eqs. (5) and (9)), the constitutive law (Eq. (3)), and the geometrical relations (not reported here, but the reader can find them in [32]), Eq. (12) adopts the following expression:

$$\delta^2(L_{int}) = \delta\mathbf{u}_{sj}^T\mathbf{K}_T^{ij\tau s}\delta\mathbf{u}_{\tau i} \tag{13}$$

In the case of stable buckling problems, the above equation can be linearized to give:

$$\delta^2(L_{int}) \cong \delta\mathbf{u}_{sj}^T(\mathbf{K}_0^{ij\tau s} + \mathbf{K}_\sigma^{ij\tau s})\delta\mathbf{u}_{\tau i} \tag{14}$$

In Eq. (13), $\mathbf{K}_T^{ij\tau s}$ is the tangent stiffness matrix written in terms of CUF 3×3 fundamental nucleus, see [32]. The fundamental nucleus is independent of the theory approximation and can be expanded against F_τ approximation ($\tau, s = 1, ..., M$) and N_i shape functions ($i, j = 1, ..., N_{elem}$) to obtain the final stiffness matrix of any high-order model, including LW. Now, the tangent stiffness matrix is expressed as $\mathbf{K}_T^{ij\tau s} = \mathbf{K}_0^{ij\tau s} + \mathbf{K}_\sigma^{ij\tau s}$, where $\mathbf{K}_0^{ij\tau s}$ is the fundamental nucleus of the linear stiffness matrix and $\mathbf{K}_\sigma^{ij\tau s}$ is the fundamental nucleus of

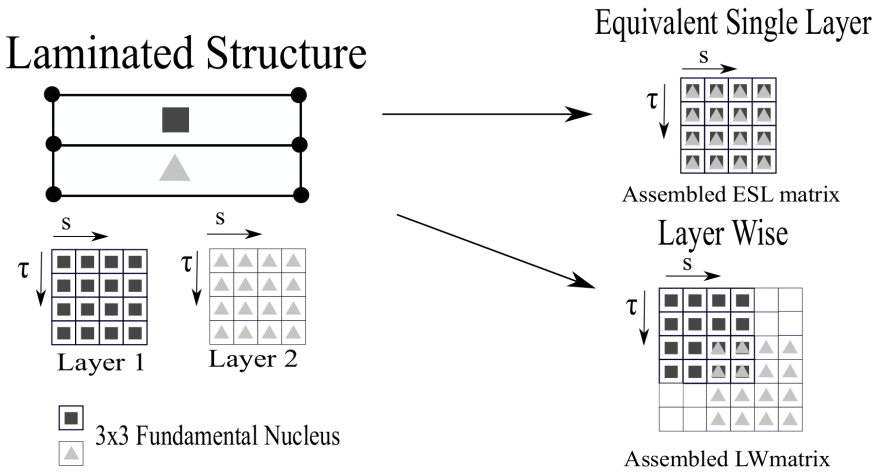

Figure 3: Assembling procedures of the stiffness matrix.

the geometric stiffness matrix. This latter contribution is strictly dependent on the internal pre-stress state within the structure. The accuracy of the model will depend on the capability to describe the internal stress state [34]. For the sake of brevity, the expression to calculate the tangent matrix is not offered here, but can be found in [35]. Note that, because linear hypothesis holds, $\mathbf{K}_\sigma$ is supposed to be proportional to λ_{cr} and Eq. (11) can be written as

$$|\mathbf{K}_0 + \lambda_{cr}\mathbf{K}_\sigma| = 0 \tag{15}$$

which provides the critical buckling load factor λ_{cr}. Note that $\mathbf{K}_0$ and $\mathbf{K}_\sigma$ represent the global assembled FE arrays.

3.1.4 Equivalent single layer vs Layerwise models

In order to analyse laminated structures, two approaches can be adopted: the equivalent single layer approach, referred to as ESL, and the layerwise approach, referred to as LW. By using ESL approach, the contribution of each layer of the laminate is summed when conforming the stiffness matrix, homogenising the properties of the different layers into a single one. The result is that the multilayer configuration is modelled as a single layer having a set of variables assumed for the entire cross-section. Note that ESL can be implemented independently of the class of CUF model (e.g. TE, LE). Obviously, the main disadvantage of ESL approach is its incapableness of correctly representing some effects inherent of each layer and their interfaces.

Conversely, in LW approach the variables of each layer are considered separately and the continuity of the displacement solutions at the interfaces between layers is assured by the correspondence of the shared sides of the cross-section expansion domains. The differences in the assembly procedure for ESL and LW are shown in Fig. 3. In this work, for merely practical reasons, ESL models are obtained by means of TE, whereas LW models are obtained by employing LE. It is worth mentioning that LW models can be obtained by means of TE, but special consideration must be given to the interface conditions in this case (see [36, 37]).

4 Random fields of fibre misalignments

All manufacturing processes present an uncertainty related to several factors, which could lead to different global properties for the late structure. In the case of VAT composite materials,

some of these factors could be variations on the mechanical properties of the material, higher or lower ply thicknesses, presence of gaps or overlaps between laminae and misalignments in the fibre orientation.

In this paper, a misalignment sensitivity analysis is carried out exploiting stochastic fields. Stochastic fields (denoted as $\boldsymbol{\theta}$), also known as random fields, are contained in $\mathbb{R}^n$, i.e. $\boldsymbol{\theta} \in \mathbb{R}^n$, and spread a parameter in space with a distribution. Each field value is correlated with the remaining components of the n-dimensional vector. There exist many methods which can be used to generate random fields and can be found in the review by Spanos [38]. For this work, Covariance Matrix Decomposition (CMD) [39] has been chosen as the employed method due to its implementation easiness and facility to vary the correlation function and length. CMD creates fields directly from an autocorrelation matrix by decomposing it and multiplying the decomposed array with a random vector. The values of the stochastic field are typically generated using a Gaussian distribution with an associated mean value, μ, and standard deviation σ. Even though misalignments might not be in such a distribution, because of the central limit theorem, they can be approximated as such with the assumption that the response is the result of many independent random variables [40].

Let us consider that points belonging to the VAT ply under consideration are correlated in space. The mathematical definition of correlation between points i and j of field $\boldsymbol{\theta}$ is

$$\rho_{\theta_i,\theta_j} = \frac{\mathrm{cov}(\theta_i, \theta_j)}{\sigma_i \sigma_j} = \frac{\mathrm{E}[(\theta_i - \mu_i)(\theta_j - \mu_j)]}{\sigma_i \sigma_j} \tag{16}$$

where E is the expectation operator used in probability and equals the mean value of a distribution given a infinite amount of samples. Eq. (16) allows to calculate the autocorrelation between points, which have to be given as input in order to generate such fields. The most common correlation functions found in the literature are based on an exponential formula [41]. In this work, the correlation function employed to generate the fields:

$$\rho = \exp\left(-\left(\frac{\Delta L}{L_c}\right)^2\right) \tag{17}$$

in which L_c is the correlation length, and ΔL is the Euclidean distance between two points. The same function was used in [26], although ΔL represented the geodesic length since curved panels were analysed. For the sake of brevity, the mathematical proof of how CMD allows reproducing stochastic fields is omitted in here but can be found in the work of van den Broek *et al.* [42].

5 Results

5.1 Validation

In this first numerical example, a twelve layer VAT laminate plate is analysed for validation purpose. This structure has been studied several times in the literature, see Gürdal *et al.* [11] or Zhou *et al.* [43]. In [11], an exhaustive analysis of VAT composite plates was carried out, by varying the different parameters involved in Eq. (1), i.e. ϕ, T_0 and T_1, and boundary conditions. As in those works, in this report two cases will be considered.

In Case I, the orientation varies along the x axis of the plate ($\phi = 0°$), which is subjected to a constant end-shortening $u_x(\pm\frac{a}{2}, y) = \mp\frac{u_0}{2}$ and restrained transverse edges, see Fig. 4. For Case II, the orientation will vary along the y axis of the plate ($\phi = 90°$), which is subjected to

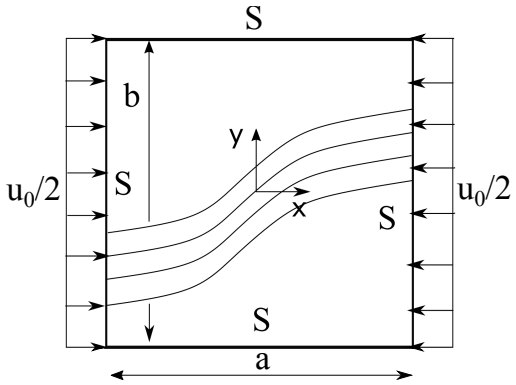

Figure 4: Geometrical properties of the plate along with boundary conditions. The structure presents two end-shortening at $x = \pm\frac{a}{2}$ and simply supported edges. Transverse edges ($y = \pm\frac{b}{2}$) are restrained for Case I lamination and free to deform for Case II lamination. S stands for simply supported edges.

a [m]	b [m]	Ply thickness [mm]	E_1 [GPa]	E_2 [GPa]	G_{12} [GPa]	ν
0.254	0.254	0.127	181	10.27	7.17	0.28

Table 1: Geometrical and material properties of the structure.

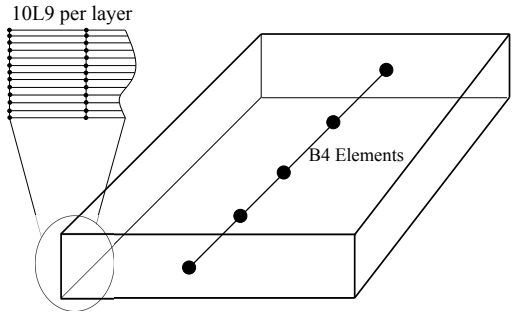

Figure 5: Numerical mesh used in the analysis, consisting in 10L9 elements per layer for the cross-section and 10B4 elements along the y-axis.

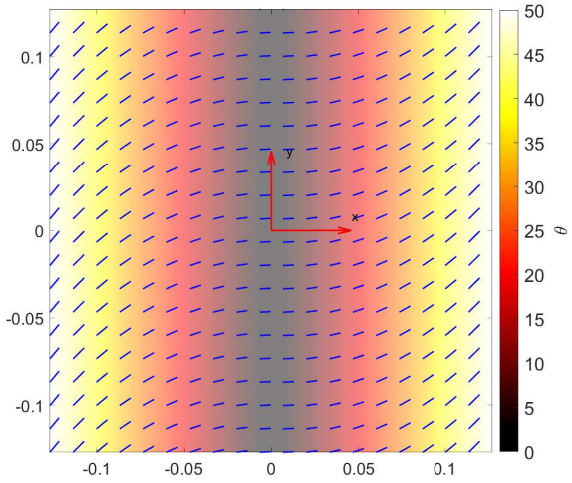

Figure 6: Case I $[0\ +<0,50>]$ fibre path. The fibre orientation angle θ [deg] is measured with regard to the x-axis.

a constant end-shortening and free transverse edges. In both cases, all the edges are simply supported. The geometrical and material properties of the plate are listed in Table 1. As shown in Fig. 5, the model used in this analysis makes use of a layerwise discretization on the VAT panel cross-section with L9 and a 1D mesh of B4 elements.

Note that, according to the proposed nomenclature from Section 2, the fibre orientations of Cases I and II can be expressed as follows:

- Case I: $[0\ \pm<0,50>]_{3s}$
- Case II: $[90\ \pm<0,75>]_{3s}$

The first ply fibre path for each case can be appreciated in Figs. 6 and 7, for representative purposes. In both cases, the fibre orientation angle is referred to the x-axis.

In reference [11], the axial stress resultant N_x are normalized by a factor a^2/E_1h^3, that is $K_{cr} = N_{cr}^{av}a^2/E_1h^3$. For Case I, the fibre orientation is only a function of the x coordinate and the in-plane stress resultant N_x is constant everywhere and reported as the critical value of the stress resultant. For Case II, on the other hand, the value of N_x depends on the y coordinate. Therefore, in order to describe the critical loading in terms of the axial stress resultant, an average of the critical load N_{cr}^{av} is defined:

$$N_{cr}^{av} = \frac{1}{b}\int_{-\frac{b}{2}}^{\frac{b}{2}} N_x(a/2,y)dy \tag{18}$$

In the performed buckling analyses, the critical buckling load F_{cr} is obtained by multiplying the first eigenvalue of the buckling problem (λ_{cr}) by the equivalent force at the shortened edges. Thus, the critical in-plane stress resultant N_{cr} is calculated by dividing the previous load by the length of the edge, b, and then normalized in order to obtain K_{cr}. The values for F_{cr} and N_{cr} from [11] were calculated backwards, that is, from K_{cr} to F_{cr}.

Before comparing the results with those available in the literature, a mesh convergence analysis depending on the number of B4 elements along the y-axis is performed for Case II lamination, see Fig. 8. The refined LW model adopted in this convergence analysis makes use of a polynomial set on the cross-section of 120 L9, that is 10 L9 per layer. The effect

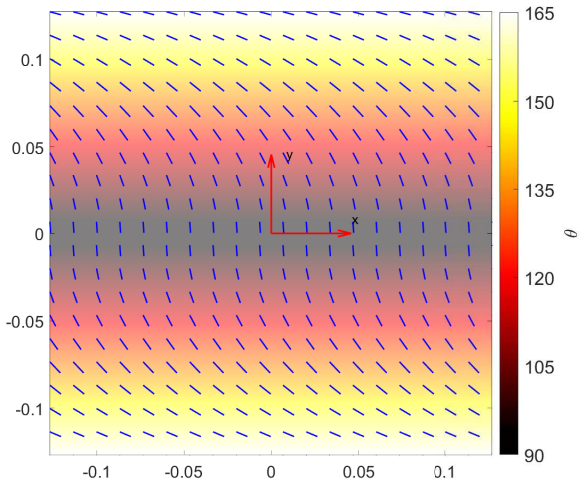

Figure 7: Case II $[90 + < 0, 75 >]$ fibre path. The fibre orientation angle θ [deg] is measured with regard to the x-axis.

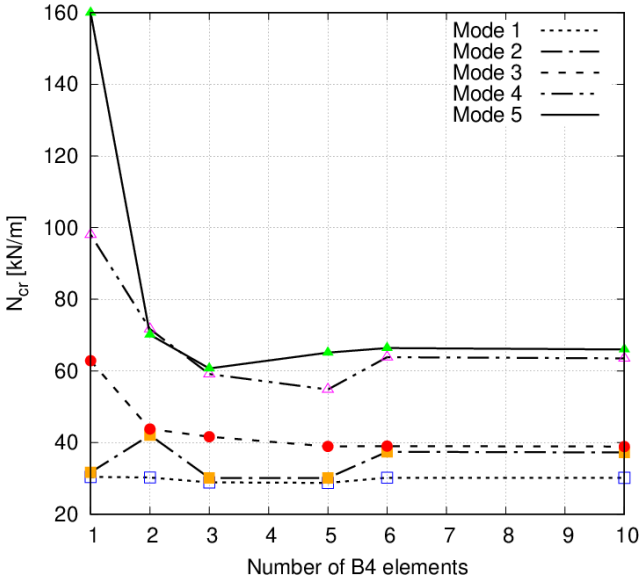

Figure 8: Mesh convergence based on the number of B4 elements along the y-axis of the $[90 \pm < 0, 75 >]_{3s}$ plate.

Case		DOF	λ_{cr} [-]	F_{cr} [kN]	N_{cr} [kN/m]	K_{cr} [-]
I	Ref [11] CLPT	$M = 15$, $N = 7$	-	3.63	14.3	1.44
	Present LW	51975	$2.25{\cdot}10^{-3}$	3.35	13.2	1.33
II	Ref [11] CLPT	$M = 7$, $N = 15$	-	7.92	31.2	3.14
	Present LW	51975	$9.84{\cdot}10^{-3}$	6.77	26.6	3.04

Table 2: Comparison between [11] and LW for Cases I and II.

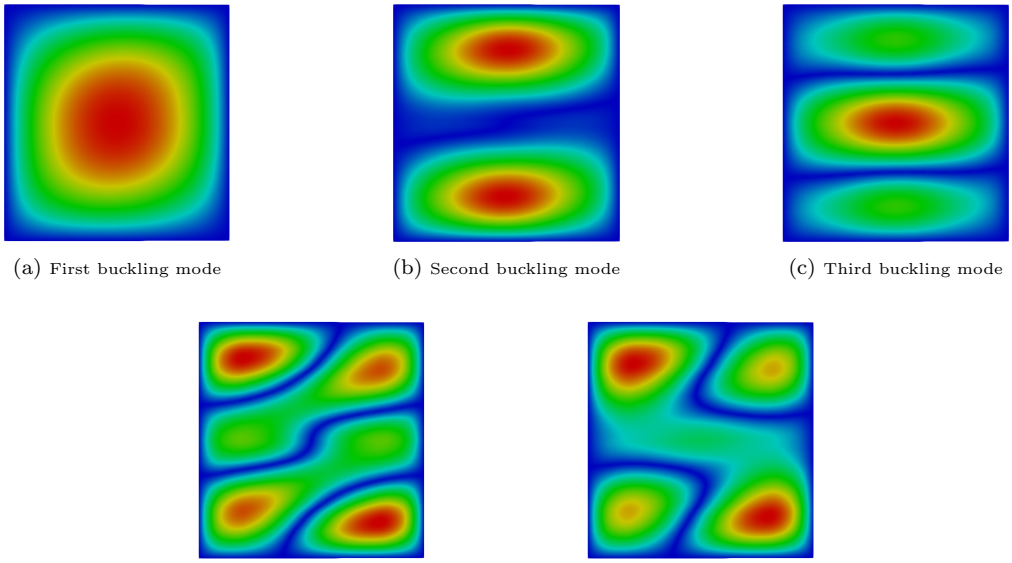

(a) First buckling mode (b) Second buckling mode (c) Third buckling mode

(d) Fourth buckling mode (e) Fifth buckling mode

Figure 9: Buckling modes of the pristine Case II VAT panel subjected to end shortening and simply supported boundary conditions.

of the theory approximation order over the discussed results is performed later in Section 5.2.2. Once the mesh is decided, a comparison between the results from [11] and the present LW model is shown in Table 2. It should be underlined that the literature results used the Classic Laminate Plate Theory (CLPT) along with Rayleigh-Ritz method to solve the buckling problem. In this case, the number of degrees of freedom (DOF) from reference are presented as the number of terms in M and N needed in the double sine series that represent the out-of-plane displacements in the Rayleigh-Ritz method. Differences in K_{cr} can be appreciated for both cases. LW models provide similar values, but slightly lower due to its capability of providing a more accurate stresses field.

Finally, for the sake of completeness, the first five buckling modes for Case II lamination are represented in Fig. 9.

5.2 Influence of fibre misalignment on buckling performance

5.2.1 Twelve-layer laminate

The influence of fibre misalignment on buckling performance of the Case II VAT plate is investigated hereafter. The misalignment of the fibre path is generated by exploiting the mathematical background depicted previously. Since a twelve layer laminate is considered, a random field is generated for each layer. Each of these fields is obtained by means of the same correlation matrix $\mathbf{R}$, since the relative distances in the laminate plane are identical for

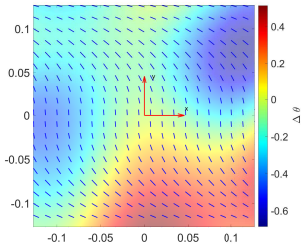

(a) Random field on a $[90+ < 0,75 >]$ ply.

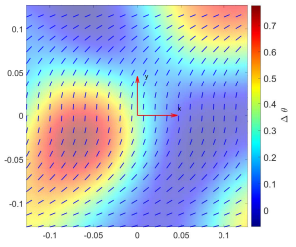

(b) Random field on a $[90- < 0,75 >]$ ply.

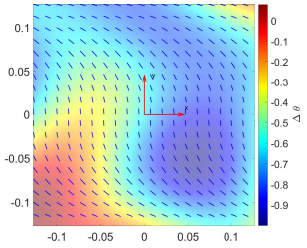

(c) Random field on a $[90+ < 0,75 >]$ ply.

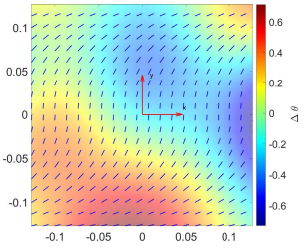

(d) Random field on a $[90- < 0,75 >]$ ply.

Figure 10: Example of 4 out of 12 randomly distributed fibre misalignment with zero mean and standard deviation of $\sigma_\theta = 0.5°$ applied on $[90 \ \pm < 0,75 >]$ plies.

each ply. Plus, one has to clarify that in this work the selected correlation length L_c depends on the rotation angle ϕ in Eq. (1), and is valued equal to the length d in the mentioned equation. Finally, a total of a thousand Monte Carlo simulations with misalignment normal distribution of zero mean and standard deviation equal to $\sigma_\theta = 0.5°$ are carried out. Some examples of misalignment random fields with zero mean and standard deviation of $\sigma_\theta = 0.5°$ applied to $[90\pm < 0,75 >]$ fibre paths are shown in Fig. 10.

The Probability Density Functions (PDFs) for the buckling load of the first five buckling modes are shown in Fig. 11. It can be observed that all the buckling loads follow a Gaussian distribution. Fig. 12 shows the Modal Assurance Criterions (MAC) matrix for the buckling problem under consideration. MAC has been used to investigate variations in the mode shapes under uncertainty. In order to determine statistics for the MAC, each mode shape, of each Monte Carlo sample, is compared with each mode shape of the pristine structure using

$$\mathrm{MAC}_{j,k}^{(i)} = \frac{|\phi_{i,j}^T \phi_{\mathrm{ref},k}|^2}{(\phi_{i,j}^T \phi_{i,j})(\phi_{\mathrm{ref},k}^T \phi_{\mathrm{ref},k})} \tag{19}$$

where $\mathrm{MAC}_{j,k}^{(i)}$ is the i^{th} sample of the j^{th} and k^{th} column of the MAC, $\phi_{i,j}$ is the j^{th} of the i^{th} sample and $\phi_{\mathrm{ref},k}$ is the k^{th} eigenvector of the reference. In detail, Fig. 12 shows the correlation between mode shapes from pristine structure and VAT laminate with defects. Note that the figure depicts both the mean MAC value and the standard deviation of each combination of buckling modes.

Table 3 summarizes the statistical properties of the critical in-plane stress resultants. It is worth mentioning that these statistics required manipulations exploiting the mean value and variance properties of random variables. Intuitively, the larger σ_θ is, the wider the buckling load PDF will result. From this standpoint, it is reasonable that a mode switching (e.g., between modes 2 and 3, or modes 4 and 5) may happen for certain values of the standard deviation of the fibre misalignment.

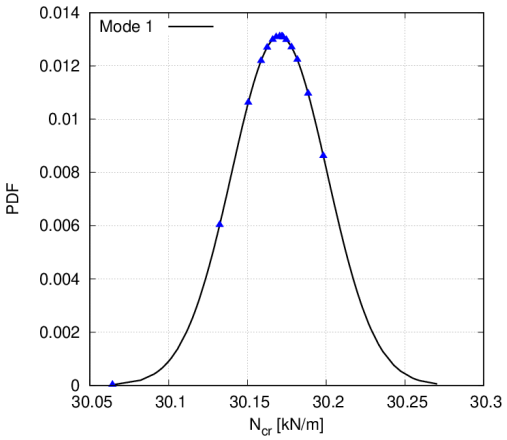

(a) PDF of Case II; first buckling load

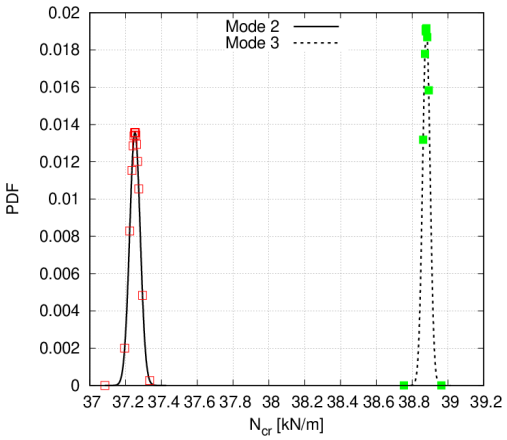

(b) PDF of Case II; second and third buckling load

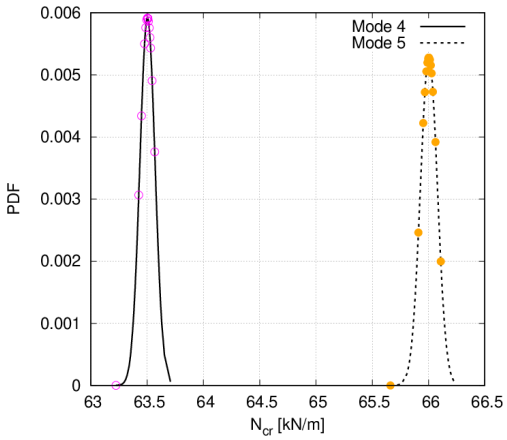

(c) PDF of Case II; fourth and fifth buckling load

Figure 11: PDF of Case II buckling loads N_{cr} presenting fibre misalignment with standard deviation equal to $\sigma_\theta = 0.5°$. Mode 1 ▲, Mode 2 □, Mode 3 ■, Mode 4 ○, Mode 5 ●.

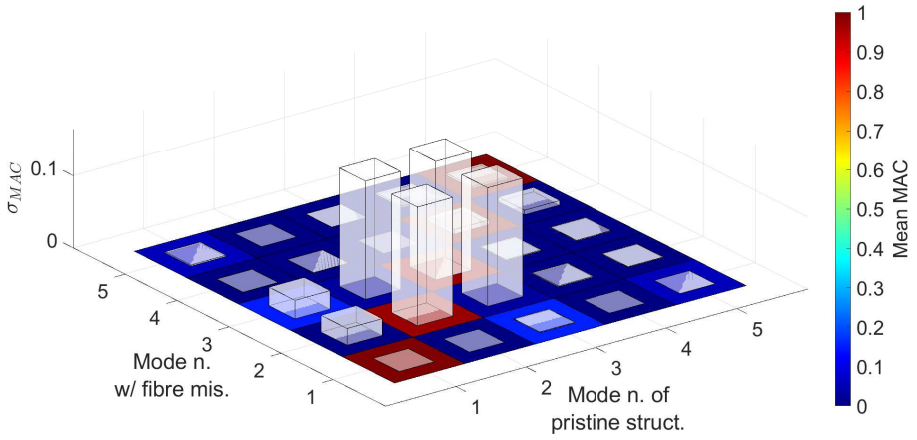

Figure 12: Mean MAC values and standard deviation between buckling modes of pristine VAT structure and defected one. The fibre misalignment field has a null mean value and standard deviation equal to $\sigma_\theta = 0.5°$. The considered lamination is: $[90\ \pm < 0, 75 >]_{3s}$.

Magnitude	Mean Value [kN/m]	Standard Deviation [N/m]
N_{cr_1}	30.17	30.41
N_{cr_2}	37.25	41.14
N_{cr_3}	38.88	36.53
N_{cr_4}	63.50	67.46
N_{cr_5}	66.00	75.64

Table 3: Statistical properties of N_{cr_i} for Case II using the proposed CUF-based LW model and statistically correlated fibre misalignment with zero mean and $\sigma_\theta = 0.5°$.

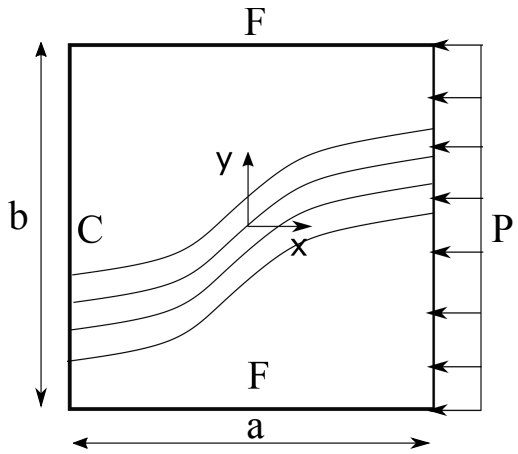

Figure 13: Boundary conditions of the $[0\ \pm < 45, 0 >]_s$ plate. C stands for clamped edge, F for free edge and P is the compression load equal to 1 N, and modelled as a distributed pressure, applied at $x = \frac{a}{2}$.

5.2.2 Effect of the structural modelling approximation

In this section we want to demonstrate the need of using a refined LW model able to model the defects at the meso-scale when conducting uncertainty analysis. For doing so, we compare the results from a low- to high-order model obtained with TE approximation and a LW model based on CUF. The structure considered in this section consists in a four-layers balanced and symmetric laminate whose stacking sequence can be expressed as: $\theta = [0\ \pm < 45, 0 >]_s$. The geometrical and material properties are the same as in Table 1. Three expansion theories are exploited: first order Taylor (TE1), third order Taylor (TE3) and Lagrange expansion, which lead respectively to an ESL and LW modelling. The scope of using these expansions is to find out if ESL theories, as those used in commercial software and classical literature, are able to predict changes in the buckling modes under fabrication uncertainties like LW formulations. For this analysis case, the plate is subjected to a compression load P, modelled as a distributed pressure over the section, equivalent to 1 N at $x = \frac{a}{2}$. Lateral edges are free, whereas one end is clamped at $x = -\frac{a}{2}$. These boundary conditions can be easily appreciated in Fig. 13. The only difference between this fibre misalignment random field and the one considered in the previous section is the standard deviation, which now values $\sigma_\theta = 1°$, remaining constant the rest of the parameters.

As mentioned in section 5.1, a cross-section mesh convergence analysis is carried out along with an *expansion* convergence analysis. Results are plotted in Figs. 14 and 15. In detail, Fig. 14 demonstrates the effect of the number of L9 subdomain on the VAT panel cross-section on the buckling loadings for the adopted LW model. It is clear that the first buckling modes

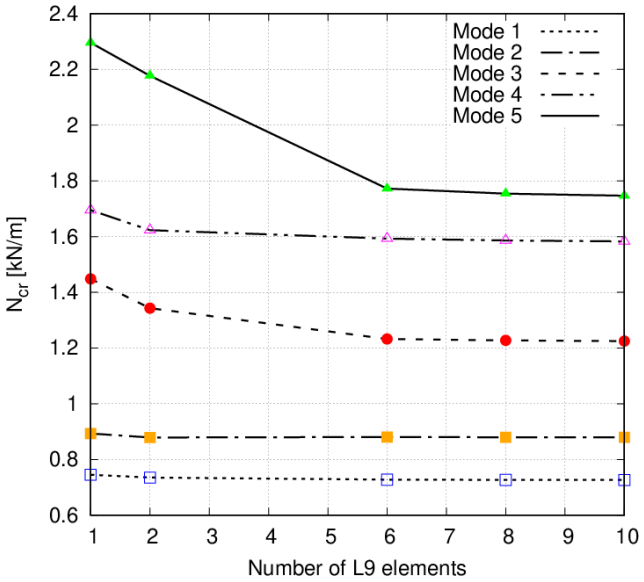

Figure 14: Convergence of the LW model against the number of ply L9 subdomains along x-axis for the $[0\ \pm < 45, 0 >]_s$ plate.

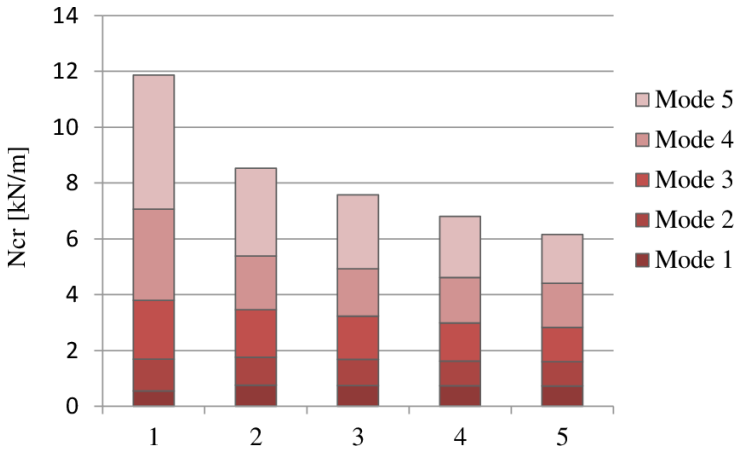

Figure 15: Comparison of the different ESL theories with LW model for the $[0\ \pm < 45, 0 >]_s$ plate. LW outcomes correspond to the 10L9 mesh from Fig. 14.

Case	Formulation	DOF	N_{cr_1} [kN/m]	N_{cr_2} [kN/m]	N_{cr_3} [kN/m]	N_{cr_4} [kN/m]	N_{cr_5} [kN/m]
$[0\ \pm < 45, 0 >]_s$	TE 1	288	0.55	1.14	2.11	3.27	4.81
	TE 3	960	0.74	0.94	1.55	1.70	2.65
	LW	18144	0.73	0.88	1.22	1.58	1.75

Table 4: N_{cr_i} comparison between ESL and LW expansions for the pristine $[0\ \pm < 45, 0 >]_s$ plate.

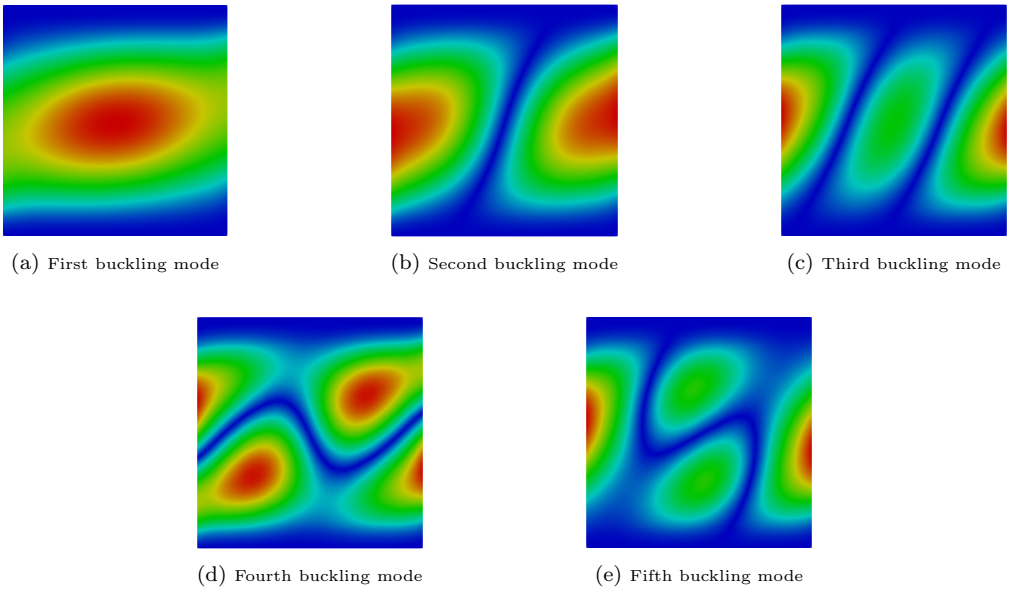

(a) First buckling mode (b) Second buckling mode (c) Third buckling mode

(d) Fourth buckling mode (e) Fifth buckling mode

Figure 16: Buckling modes of the pristine $[0\ \pm < 45, 0 >]_s$ panel with clamped-free boundary conditions using LW formulation.

are not affected by this parameter. In contrast, higher modes require a refined approximation of the LW theory kinematics, as expected. In contrast, Fig. 15 shows the differences in the buckling loads resulting from different ESL theory approximation orders, which are compared with the reference LW results. Note that higher modes are affected by severe errors when lower order models are used.

The resulting first five buckling loads for the pristine structure using the chosen expansions are summarized in Table 4 and the respective buckling modes are shown in Figs. 16 to 18. Obvious differences can be appreciated, especially those regarding the buckling modes where TE1 is unable to predict the bending-torsional couplings, since it corresponds to a simple Timoshenko beam model. Conversely, TE3 provides similar results for the first, second, third and fifth modes.

Uncertainty analysis is performed through a thousand Monte Carlo simulations, which guaranteee the correct characterization of the influence of fibre misalignments on the buckling

	TE1		TE3		LW	
	Mean [kN/m]	Std. Dev. [N/m]	Mean [kN/m]	Std. Dev. [N/m]	Mean [kN/m]	Std. Dev. [N/m]
N_{cr_1}	0.55	4.64	0.74	4.08	0.73	5.14
N_{cr_2}	1.14	14.35	0.94	5.03	0.88	4.96
N_{cr_3}	2.11	23.82	1.55	8.32	1.22	7.19
N_{cr_4}	3.27	37.76	1.70	9.01	1.58	10.68
N_{cr_5}	4.80	54.78	2.53	60.38	1.75	9.84

Table 5: Mean value and Standard deviation of N_{cr_i} for $[0\ \pm < 45, 0 >]_s$ VAT plate using TE1, TE3 and LW expansions.

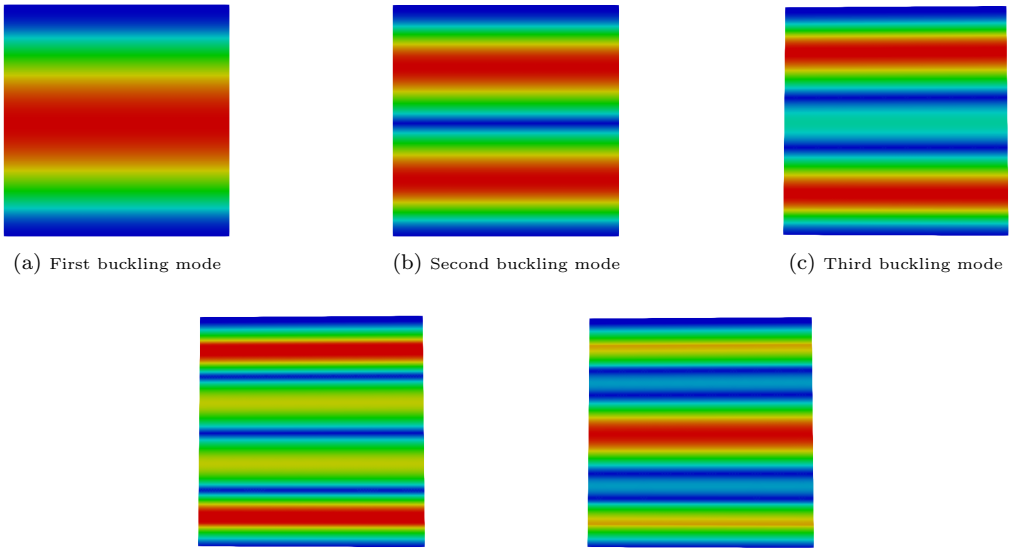

(a) First buckling mode (b) Second buckling mode (c) Third buckling mode

(d) Fourth buckling mode (e) Fifth buckling mode

Figure 17: Buckling modes of the pristine $[0 \pm < 45, 0 >]_s$ panel with clamped-free boundary conditions using TE1 formulation.

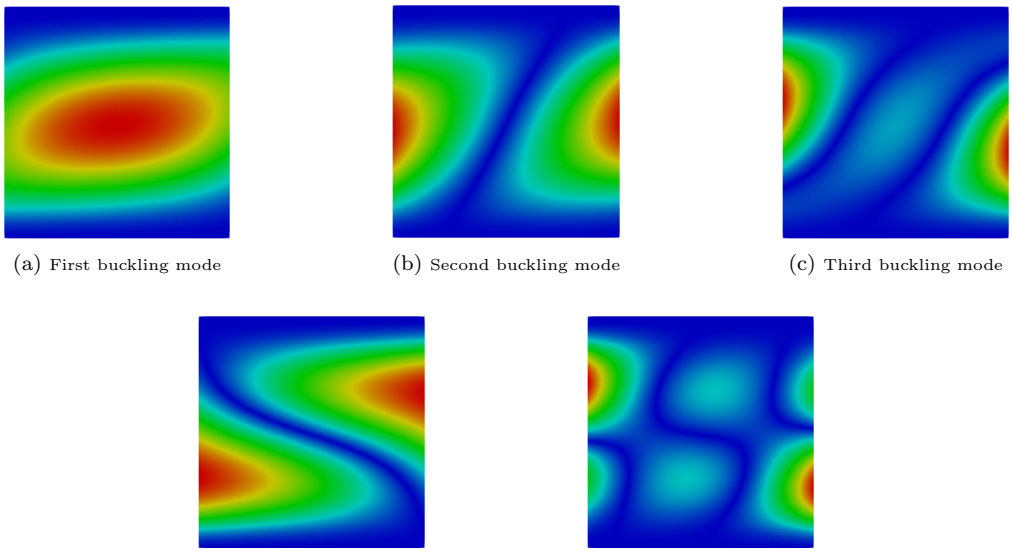

(a) First buckling mode (b) Second buckling mode (c) Third buckling mode

(d) Fourth buckling mode (e) Fifth buckling mode

Figure 18: Buckling modes of the pristine $[0 \pm < 45, 0 >]_s$ VAT panel with clamped-free boundary conditions using TE3 formulation.

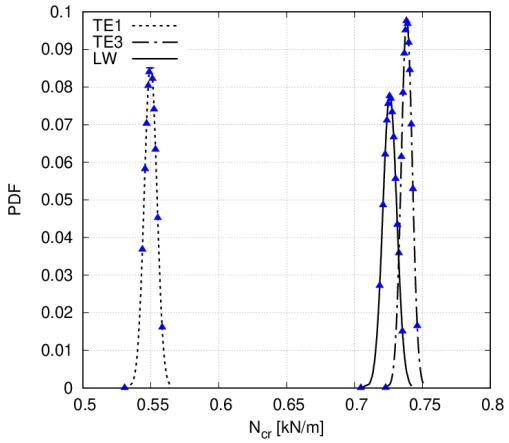

(a) PDF of first buckling load

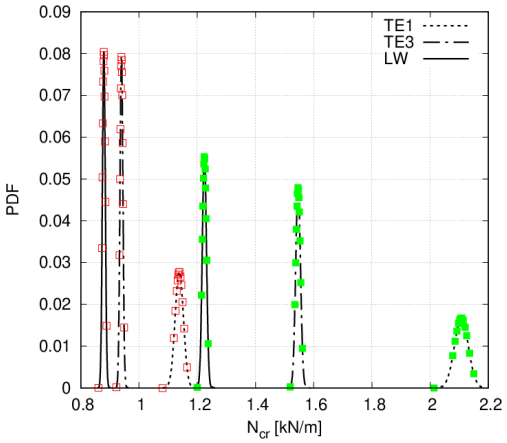

(b) PDF of second and third buckling load

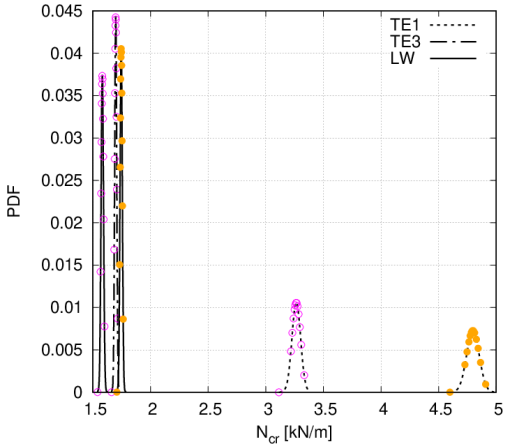

(c) PDF of fourth and fifth buckling load

Figure 19: PDF of buckling loads N_{cr_i} for the $[0\ \pm < 45, 0 >]_s$ VAT plate presenting fibre misalignment with standard deviation equal to $\sigma_\theta = 1^\circ$ employing TE 1, TE 3 and LW expansions. Mode 1 ▲, Mode 2 □, Mode 3 ■, Mode 4 ○, Mode 5 •

performance. The resulting mean values and standard deviations for the buckling loads according to the different theories are listed in Table 5. It can be appreciated that TE3 provides accurate results for the first buckling load, yet still overestimates the remaining buckling loads with regard to LW. However, it is remarkable the fact that TE3 and LW standard deviations are quite similar, except for the fifth load.

PDFs of the buckling loads N_{cr_i} are displayed in Fig. 19. Note that the figure does not present the fifth buckling load by TE3 because it does not show a normal distribution. Nevertheless, Fig. 19c, along with MAC criterion in Fig. 20, which is given here for each theory approximation, proves that LW is able to catch the eventual resemblances between modes of the flawed structure and the pristine modes. Additionally, if a larger misalignment standard deviation had been considered, a possible mode switching between the fourth and fifth mode would have been captured.

Regarding the fifth TE3 buckling load, Fig. 20b provides that the mean value for $\text{MAC}_{5,5}$ is nearly 0.2, while $\text{MAC}_{2,5}$ and $\text{MAC}_{4,5}$ mean values are respectively 0.6 and 0.35. PDF of the latter are plotted in Fig.21a, while the former is displayed using a histogram for a better visualisation in Fig. 21b. The histogram shows that nearly 23% of the samples are gathered around $\text{MAC}_{5,5} \approx 1$, which corresponds to $N_{cr_5} \approx 2.65$ kN/m, whilst the remaining 77%

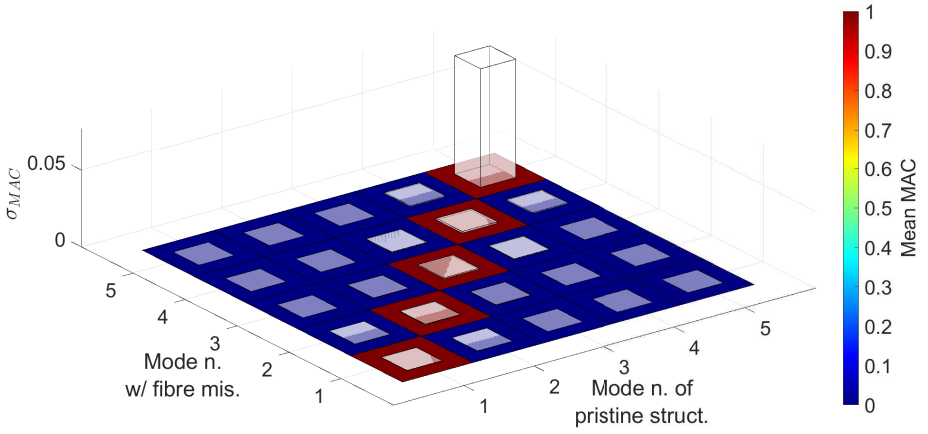

(a) MAC criterion using TE1

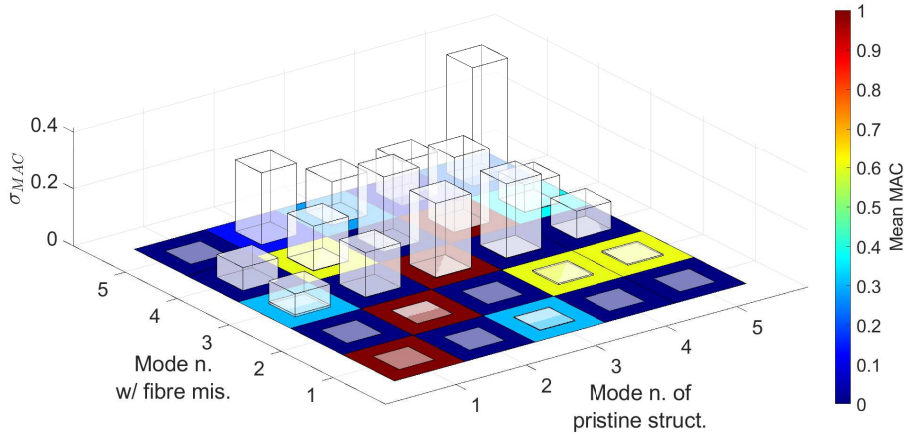

(b) MAC criterion using TE3

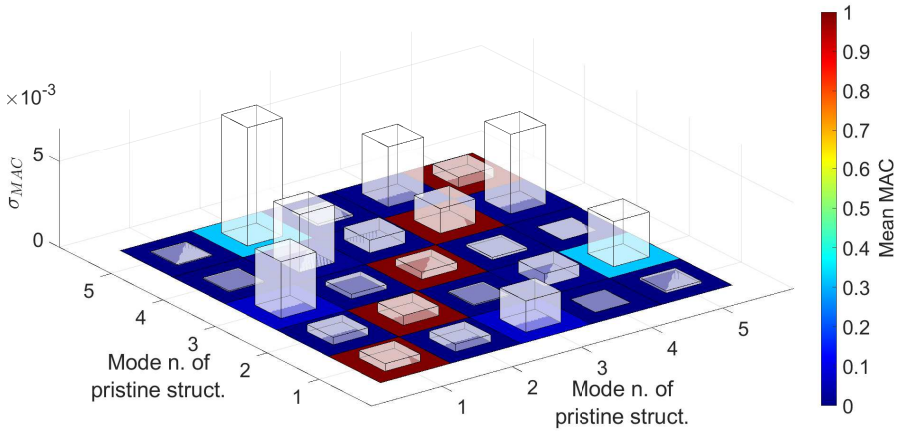

(c) MAC criterion using LW

Figure 20: Mean MAC values and standard deviation between buckling modes of pristine VAT panel and defected one employing TE1, TE3 and LW expansions. The fibre misalignment field has a null mean and standard deviation equal to $\sigma_\theta = 1°$. The considered lamination is $[0\ \pm < 45, 0 >]_s$.

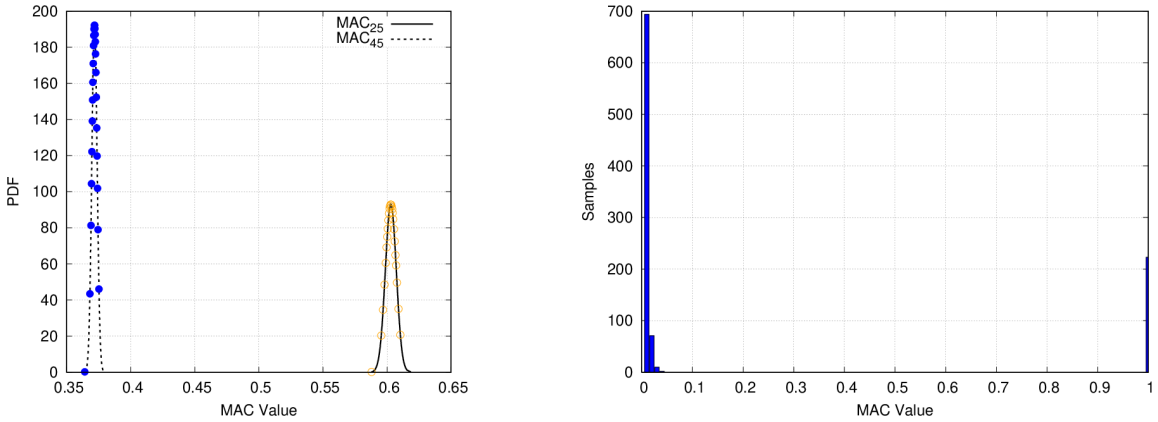

(a) $MAC_{2,5}$ and $MAC_{4,5}$ PDFs

(b) $MAC_{5,5}$ histogram

Figure 21: (a) PDF of MAC criterion indexes $MAC_{2,5}$ and $MAC_{4,5}$ and (b) $MAC_{5,5}$ histogram divided into 0.01 bins. Both the figures correspond to the TE3 expansion analysis of the $[0 \pm < 45, 0 >]_s$ VAT panel.

approximately equals 0 and its buckling load is around $N_{cr_5} \approx 2.50$ kN/m. This means that when fibre misalignments are taken into account TE3 not only overestimates higher buckling loads, but also may alter the respective buckling mode.

6 Conclusion

In this work, a higher-order model based on the Carrera Unified Formulation (CUF) has been used for the linearised buckling analysis of plates made of VAT composites with fibre misalignments. Two balanced and symmetric plates with twelve layers widely studied in literature have been analysed for validation of the model and similar results have been obtained. Differences between reference and those presented in this work are due to the nature of the employed formulation. In particular, it is demonstrated that, when a layerwise (LW) formulation is employed, a more accurate estimation of the buckling can be guaranteed because pre-stress state is correctly foreseen.

Based on a LW structural model, the influence of fibre misalignments on the buckling performances of VAT panel has been carried out by means of Monte Carlo analyses. Fibre misalignments following a Gaussian distribution of zero mean and 0.5 degrees standard deviation have been modelled by means of stochastic fields generated by exploiting the covariance matrix decomposition method. The results have shown that the buckling loadings and modes hold a Gaussian distribution. In particular, it is reasonable to underline that mode switching may happen in the case of severe defects.

Particular attention has been focussed on the effect of the structural formulation in the characterization of the uncertainty. The results have shown, indeed, that layerwise models are strictly mandatory when sensitivity analysis versus meso-scale flaws is accounted for. As a matter of fact, classical structural theories based on an equivalent single layer approximation may lead to misleading results, both in the simulation of the pristine VAT structure and the defected one.

7 Acknowledgements

This work is part of a project that has received funding from the European Research Council (ERC) under the European Union's Horizon 2020 research and innovation programme (Grant agreement No. 850437).

References

[1] D.D.L. Chung. *Tailoring Composite Materials*, pages 157–201. Springer London, London, 2010.

[2] S.B. Biggers and S. Srinivasan. Compression buckling response of tailored rectangular composite plates. *AIAA Journal*, 31:590–596, 1993.

[3] S.B. Biggers and S.S. Pageau. Shear buckling response of tailored composite plates. *AIAA Journal*, 32(5):1100–1103, 1994.

[4] N.V. Banichuk. Optimization problems for elastic anisotropic bodies. *Archive of Mechanics*, 33(6):347–363, 1981.

[5] N.V. Banichuk, V.V. Sarin, and A.A. Barsuk. Optimal orientation of orthotropic materials for paltes designed against buckling. *Structural Optimization*, 10:191–196, 1995.

[6] P. Pedersen. On thickness and orientational design with orthotropic materials. *Structural Optimization*, 3:69–78, 1991.

[7] P. Pedersen. *Optimal Orientation of Anisotropic Materials Optimal Distribution of Anisotropic Materials Optimal Shape Design with Anisotropic Materials Optimal Design for a Class of Non-Linear Elasticity*, pages 649–681. Springer Netherlands, 1993.

[8] G. Duvaut, G. Terrel, F. Léné, and V.E. Verijenko. Optimization of fiber reinforced composites. *Composite Structures*, 48:83–89, 2000.

[9] Z. Gürdal and R. Olmedo. In-plane response of laminates with spatially varying fiber orientations - variable stiffness concept. *AIAA Journal*, 31(4):751–758, 1993.

[10] Z. Gürdal and R. Olmedo. Buckling response of laminates with spatially varying fiber orientations. In *34th Structures, Structural Dynamics and Materials Conference*, La Jolla, California, USA, 1993. AIAA.

[11] Z. Gürdal, B.F. Tatting, and K. Wu. Variable stiffness composite panels: Effects of stiffness variation on the in-plane and buckling response. *Composites Part A: Applied Science and Manufacturing*, 39:911–922, 2008.

[12] A.W. Blom, C.S. Lopes, P.J. Kromwijk, Z. Gurdal, and P.P. Camanho. A theoretical model to study the influence of tow-drop areas on the stiffness and strength of variable-stiffness laminates. *Journal of Composite Materials*, 43(5):403–425, 2009.

[13] K. Kazem Fayazbakhsh, M.A. Nik, D. Pasini, and L. Lessard. Defect layer method to capture effect of gaps and overlaps in variable stiffness laminates made by automated fiber placement. *Composite Structures*, 97:245–251, 2013.

[14] M.A. Nik, K. Kazem Fayazbakhsh, D. Pasini, and L. Lessard. Optimization of variable stiffness composites with embedded defects induced by automated fiber placement. *Composite Structures*, 107:160–166, 2014.

[15] K. C. Wu, B. Farrokh, B. Stanford, and P. Weaver. Imperfection insensitivity analyses of advanced composite tow-steered shells. In *57th AIAA/ASCE/AHS/ASC Structures, Structural Dynamics, and Materials Conference*, page 1498, San Diego, California, USA, 2016.

[16] E Carrera. Theories and finite elements for multilayered anisotropic, composite plates and shells: a unified compact formulation with numerical assessment and benchmarking. *Archives of Computational Methods in Engineering*, 10(3):216–296, 2003.

[17] E Carrera and G. Giunta. Refined beam theories based on carrera's unified formulation. *International Journal of Applied Mechanics*, 2(1):117–143, 2010.

[18] E Carrera, G. Giunta, P. Nali, and M. Petrolo. Refined beam elements with arbitrary cross-section geometries. *Computers and Structures*, 88(5):283 – 293, 2010.

[19] E. Carrera, M. Filippi, and E. Zappino. Laminated beam analysis by polynomial, trigonometric, exponential and zig-zag theories. *European Journal of Mechanics-A/Solids*, 41:58–69, 2013.

[20] L. Demasi, G. Biagini, F. Vannucci, E. Santarpia, and R. Cavallaro. Equivalent single layer, zig-zag, and layer wise theories for variable angle tow composites based on the generalized unified formulation. *Composite Structures*, 177:54–79, 2017.

[21] L. Demasi, G. Biagini, F. Vannucci, E. Santarpia, and R. Cavallaro. Generalized unified formulation - based bending analysis of variable angle tow panels in the presence of hole. In *2018 AIAA/ASCE/AHS/ASC Structures, Structural Dynamics, and Materials Conference*, Kissimmeee, Florida, USA, 2018. AIAA.

[22] A. Viglietti, E. Zappino, and E. Carrera. Analysis of variable angle tow composites structures using variable kinematic models. *Composites Part B: Engineering*, 171:272–283, 2019.

[23] G.I. Schüeller. Developments in stochastic structural mechanics. *Archive of Applied Mechanics*, 75:755–773, 2006.

[24] C. Bucher. Applications of random field models in stochastic structural mechanics. In *Advances in Engineering Structures, Mechanics & Construction*, pages 471–484. Springer, Berlin, Germany, 2006.

[25] S. Mukherjee, R. Ganguli, and S. Gopalakrishnan. Optimization of laminated composite structure considering uncertainty effects. *Mechanics of Advanced Materials and Structures*, 26(6):493–502, 2019.

[26] C. Scarth, S. Adhikari, P. Cabral, G. Silva, and A. Prado. Random field simulation over curved surfaces: Applications to computational structural mechanics. *Computer Methods in Applied Mechanics and Engineering*, 345:283–301, 2019.

[27] J.N. Reddy. *Mechanics of Laminated Composite Plates and Shells: Theory and Analysis*. CRC Press, Boca Raton, Florida, USA, 2004.

[28] A. Pagani, A.G. de Miguel, M. Petrolo, and E. Carrera. Analysis of laminated beams via unified formulation and Legendre polynomial expansions. *Composite Structures*, 156:78–92, 2016. 70th Anniversary of Professor J. N. Reddy.

[29] E. Carrera, A. Pagani, and M. Petrolo. Component-wise method applied to vibration of wing structures. *Journal of Applied Mechanics*, 80(4):15, 2013.

[30] E. Carrera and A. Pagani. Free vibration analysis of civil engineering structures by component-wise models. *Journal of Sound and Vibration*, 333:4597–4620, 2014.

[31] E. Carrera, A. Pagani, M. Petrolo, and E. Zappino. Recent developments on refined theories for beams with applications. *Mechanical Engineering Reviews*, 2(2), 2015.

[32] E. Carrera, M. Cinefra, M. Petrolo, and E. Zappino. *Finite Element Analysis of Structures through Unified Formulation*. Wiley, Hoboken, New Jersey, USA, 2014.

[33] E. Carrera and M. Petrolo. Refined beam elements with only displacement variables and plate/shell capabilities. *Meccanica*, 47(3):537–556, 2012.

[34] E. Carrera. Cz0 requirements: models for the two dimensional analysis of multilayered structures. *Composite Structures*, 37(3):373–383, 1997.

[35] B. Wu, A. Pagani, W. Q. Chen, and E. Carrera. Geometrically nonlinear refined shell theories by carrera unified formulation. *Mechanics of Advanced Materials and Structures*, pages 1–21, 2019.

[36] E. Carrera, A. Pagani, and M. Petrolo. Use of Lagrange multipliers to combine 1d variable kinematic finite elements. *Computers and Structures*, 129:194–206, 2013.

[37] E. Carrera and A. Pagani. Multi-line enhanced beam model for the analysis of laminated composite structures. *Composites Part B: Engineering*, 57:112–119, 2014.

[38] P.D. Spanos and B.A. Zeldin. Monte carlo treatment of random fields: A broad perspective. *Applied Mechanics Reviews*, 51(3):219–237, 1998.

[39] M.W. Davis. Production of conditional simulations via the lu triangular decomposition of the covariance matrix. *Mathematical Geology*, 19:91–98, 1987.

[40] E. Vanmarcke. *Random Fields: Analysis and Synthesis*. World Scientific, Singapore, 2010.

[41] S. van den Broek, S. Minera, A. Pirrera, P. Weaver, E. Jansen, and R. Rolfes. Enhanced deterministic performance of panels using stochastic variations of geometric and material parameters. In *AIAA Scitech 2019 Forum*, San Diego, California, USA, January 2019.

[42] S. van den Broek, S. Minera, A. Pirrera, P. Weaver, E. Jansen, and R. Rolfes. Enhanced deterministic performance of panels using stochastic variations of geometry and material. *AIAA Journal*, 58(5):2307–2320, 2020.

[43] X. Zhou and P. Gosling. Towards an understanding of variations in the buckling tailored variable angle tow composite plates. *Composite Structures*, 203:797–809, 2018.